



# Recurrence analysis of phase distribution changes during boiling flow in parallel minichannels

Gabriela Rafalko<sup>1,a</sup>, Hubert Grzybowski<sup>1</sup>, Paweł Dzienis<sup>1</sup>, Iwona Zaborowska<sup>1</sup>, Romuald Mosdorf<sup>1</sup>, and Grzegorz Litak<sup>2</sup>

<sup>1</sup> Faculty of Mechanical Engineering, Białystok University of Technology, Wiejska 45 C, 15-351 Białystok, Poland

<sup>2</sup> Department of Applied Mechanics, Lublin University of Technology, Nadbystrzycka 36, 20-618 Lublin, Poland

Received 29 June 2022 / Accepted 29 November 2022 / Published online 15 December 2022  
© The Author(s) 2022

**Abstract** In the paper, flow boiling in three parallel minichannels with a common inlet and outlet area was examined. The synchronization between flow distributions in minichannels was analyzed in local area (image analysis) and as the process of the synchronization between inlet and outlet pressure fluctuations. These processes were studied using cross recurrence plot. The analysis of pixel brightness changes inside minichannels has been applied to identify the similarity of flow patterns changes inside minichannels. The results have revealed that the processes of synchronization have a negative impact on water inlet and outlet temperature and inlet and outlet pressure oscillations. During synchronization high amplitude of oscillations of temperature and pressure occur. The mentioned behaviors are caused mainly by reverse flow. In the paper it has been shown that recurrence analysis of inlet and outlet pressure oscillations can be used for assessment of boiling synchronization in minichannels.

## 1 Introduction

In the systems with parallel minichannels dynamic instabilities are accompanied by synchronization of processes in neighboring minichannels: temperature fluctuations [1], pressure oscillations [2] and changes of two-phase flow patterns [3]. Two-phase flow instabilities are related to periodic or non-periodic oscillations of heat and mass transfer [4]. In heat-exchangers with minichannels, a thinner gap between the channels and a common inlet area induce the processes of synchronization [5].

Recent advantages in technology have led to a greater attention given to investigations of the performance of mini/microchannel devices. Two-phase flow in mini/microchannel is characterized with ability to remove large amount of heat in a limited space. However, maldistribution during these processes is observed, which reduces thermal and hydraulic performance [6]. Research is still being carried out in order to investigate and control the occurring maldistribution (e.g., non-uniform heating, flow maldistribution, uneven pressure distribution) [7–9].

In the paper, flow boiling in three parallel minichannels with a common inlet area was examined using cross recurrence plot (CRP). A qualitative analysis of

CRPs considering only diagonal lines was performed by applying the diagonal cross-recurrence profile analysis (DCRP) [10]. The synchronization between flow distributions in minichannels was analyzed in local area (image analysis) and as the process of the synchronization between inlet and outlet pressure fluctuations. An asymmetry of synchronization between pairs of channel was observed. Such asymmetry is a result of the heat-exchanger construction based on two parts: one made of copper, the second—out of Teflon. This geometry was designed in such a way to avoid heating the water in the common inlet plenum. In such construction the axis of common inlet plenum cannot be equally positioned with the axis of the middle channel (because of O-rings usage). The results have revealed that the processes of synchronization have a negative impact on water inlet and outlet temperature and inlet and outlet pressure oscillations. The mentioned phenomena are caused mainly by reverse flow. In the paper it has been shown that recurrence analysis of inlet and outlet pressure oscillations can be used for assessment of boiling synchronization in minichannels.

<sup>a</sup> e-mail: [rafalkogabriela@gmail.com](mailto:rafalkogabriela@gmail.com) (corresponding author)

## 2 Experimental setup and data characteristics

In Fig. 1, the experimental setup and an example frame of the recorded video are presented. The heat-exchanger with three parallel minichannels was heated using electric power (Fig. 1a— $q_{\text{sup}}$ ). The positioning of the minichannel element was based on O-rings. A vertical row of three K-type thermocouples was installed under minichannels in the copper block (Fig. 1a— $T_1$ ,  $T_2$ ,  $T_3$ ). The internal dimensions of minichannels were equal to 0.25 mm (width)  $\times$  0.50 mm (depth) and 32 mm (length) (the wall between the channels: 0.25 mm wide). The minichannels were covered with a plexi cover which allowed observations of flow boiling inside minichannels. The high speed camera (Fig. 1a—8) was used to record flow patterns inside minichannels. The videos were recorded at the speed of 2000 fps. The working liquid was distilled water. A gear pump (Fig. 1a—1) was used to pump the water to the compressible volume tank (Fig. 1a—2). A Coriolis mass flow meter (Fig. 1a—3) was used to measure the water mass flow rate.

The thermocouples (Fig. 1a— $T_{\text{in}}$ ,  $T_{\text{out}}$ ) were placed in the water inlet and outlet common area. The pressure sensors were used to measure the pressure in inlet and outlet common area (Fig. 1a—4, 6). Two data acquisition systems were used to record all signals with a frequency of 1 kHz. The registration of signals and films was synchronized. The system did not contain any automatic systems to control the mass and heat flux, therefore, the pressure oscillations generated during the

experiment were related to the studied phenomenon of flow boiling.

During the experiment the electric power was constant, but the water flow rate was changing in the range of:  $\dot{m} = 175\text{--}570$  g/h. The average heat flux ( $q$ ) vs. water flow rate ( $\dot{m}$ ) is shown in Fig. 2, where a 3rd degree polynomial was used to approximate the values of the average heat flux. When the water flow rate was low, the boiling was intense and the values of heat flux were high. With the increase in water flow rate, the decrease in heat flux was observed (the boiling was less intense).

In Table 1, the examples of different flow patterns observed near the inlet common area were presented. When the water flow rate was low, the boiling was intense and a higher content of vapor in the channels was observed ( $\dot{m} = 175$  g/h). We have also observed vapor reverse flow in the inlet common area which created vapor bubbles in this area ( $\dot{m} = 175$  g/h,  $\dot{m} = 348$  g/h). With the increase in water flow rate ( $\dot{m} = 383$  g/h), the fragmentation of vapor slugs occurred and the amount of liquid in minichannels was increasing. Short slugs and vapor bubbles were filling the minichannels near the inlet area ( $\dot{m} = 383$  g/h). During less intense boiling the changes of flow patterns occurred more rarely, a higher content of liquid phase was observed in the channels ( $\dot{m} = 472$  g/h).

An analysis of pixel brightness changes near the inlet area based on the experimental data gathered in the same experimental setup (Fig. 1) has been previously performed [11]. The authors have observed that during intense boiling reverse flow occurred which resulted in a formation of vapour bubbles in the inlet area (which

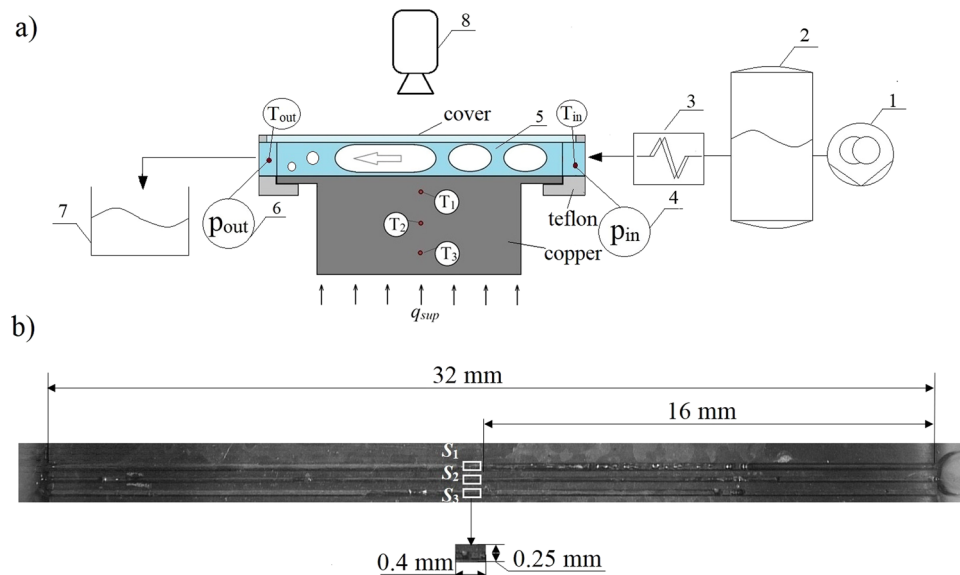


**Fig. 1** The experimental setup: **a** the test section, 1—gear pump (Tuthill model DGS.11), 2—compressible volume (volume: 222.8 cm<sup>3</sup>),  $q_{\text{sup}}$ —heating power ( $q_{\text{sup}} = 36.75$  W), 3—Coriolis mass flow meter (Bronkhorst mini CORI-FLOW™ M13; accuracy of  $\pm 0.2\%$  of rate),  $T_1, T_2, T_3, T_{\text{in}}, T_{\text{out}}$ —thermocouples (type K, 1 mm diameter, accuracy:  $\pm 2.5$  °C), 4, 6—pressure sensors (MPX5010DP, time response: 1 ms), 5—three parallel minichannels (dimensions: 32.00 mm  $\times$  0.25 mm  $\times$  0.50 mm), 7—outlet tank, 8—high speed camera (Phantom v1610); **b** the scheme of visual data analysis,  $S_1, S_2, S_3$ —the sum of pixel brightness in the analyzed parts of minichannels number 1, 2, 3, respectively

**Fig. 2** Mean values of heat flux ( $q$ ) vs. water flow rate ( $\dot{m}$ ) and the 3rd degree polynomial approximation

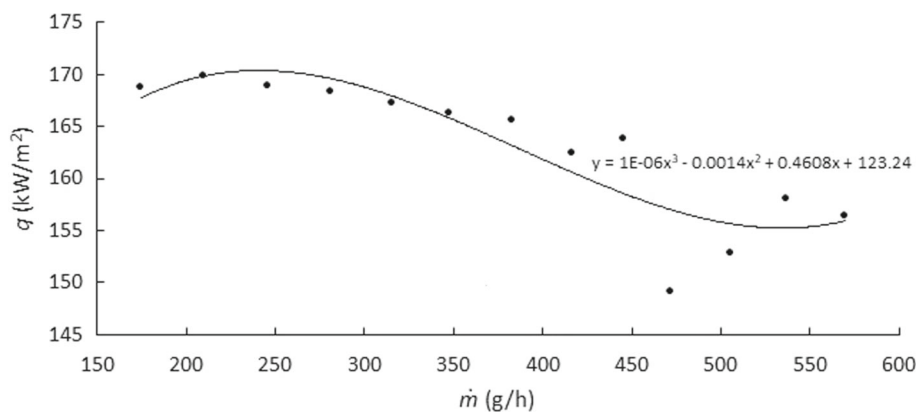


**Table 1** Flow characteristics based on visual observations

water flow rate ( $\dot{m}$ ) (g/h)	flow patterns (visual observations)	an example of a video frame
175	long vapour slugs, small vapour bubbles, a higher content of vapour, reverse flow	
348	short vapour slugs, numerous vapour bubbles, reverse flow, reverse flow	
383	slugs fragmentation, increasing amount of liquid	
472	higher content of liquid, vapour bubbles, short slugs	

will be further called as ‘reverse flow bubbles’—RFB). The creation and movement of the RFB influenced flow patterns observed in minichannels near the inlet area. During intense boiling, the RFB were created (oscillated) almost periodically in the inlet area and pushed back into minichannels. This caused the occurrence of rather long vapour slugs in minichannels (Table 1,  $\dot{m} = 175$  g/h). During less intense boiling, the RFB were created rather separately on each minichannel. Rarely, vapour from RFB was pushed back into minichannels and this way small vapour bubbles and short slugs were filling the minichannels (Table 1,  $\dot{m} > 383$  g/h).

**2.1 Phase distribution during boiling flow**

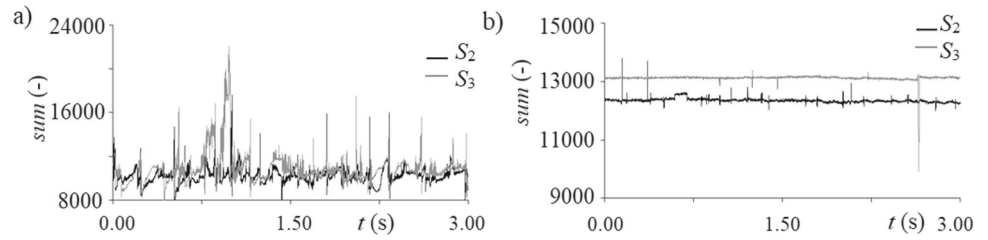
In order to analyze the changes of phase distribution in minichannels, the pixel brightness in the middle part of each minichannel was summed in the area (called ‘gates’) denoted in Fig. 1b with the letter  $S$ , located 16 mm away from the inlet area. When the vapor was filling minichannel the pixel brightness was lower than in case of liquid occurrence in the channel. However, the front of vapor slugs was often represented by white pixels (light reflection occurred).

The dimensions of the gates were following: 0.40 mm  $\times$  0.25 mm. The width of the gate corresponded to the

width of minichannel while the length of the gate corresponded to the length of a short slug. The sum of pixel brightness indicated the phase distribution (presence of vapor or water) at a particular time. In Fig. 3a pixel brightness changes (sum) in two minichannels during very intense boiling in function of time were presented. High oscillations of pixel brightness changes correspond to the occurrence of short and long vapor slugs which fronts reflect the light during the experiment. Figure 3b shows pixel brightness changes in two neighboring minichannels during less intense boiling. In Fig. 3b a rather constant level of pixel brightness corresponds to the occurrence of liquid flow in the analyzed part of minichannel.

Due to small dimensions of the analyzed parts of minichannels (0.4 mm  $\times$  0.25 mm) the calculated sum of pixel brightness is directly related to the changes of phase distribution in the gates. In order to quantitatively analyze the phase distribution changes and the process of flow synchronization in the parts of neighboring minichannels, the Diagonal Cross-Recurrence Profile (DCRP) Analysis was applied [12]. We have applied the CRP algorithm to the recorded visual data in order to benchmark the similarity of the states occurring in parallel minichannels during flow boiling.

**Fig. 3** The pixel brightness changes vs. time in two parallel minichannels (2, 3): **a**  $\dot{m} = 175$  g/h, **b**  $\dot{m} = 505$  g/h



2.1.1 Diagonal cross-recurrence profile (DCRP) analysis

The cross recurrence plot (CRP) is a special variation of the recurrence plot. Compared to a recurrence plot, the CRP is used to describe the similarity between the states of two dynamical systems  $x_i$  and  $y_j$  ( $i = 1, \dots, N$ ;  $j = 1, \dots, M$ ) which are embedded in the same phase space.

Cross recurrence plot is a matrix with dimensions  $N \times M$  and is described by the following relationship [13]:

$$CRP_{i,j}^m = \Theta(\varepsilon_i - x_i - y_j), i = 1, \dots, N, j = 1, \dots, M, \tag{1}$$

where  $\Theta$ —Heaviside step function,  $\varepsilon$ —a diameter of the sphere inside which the distance of two points is tested,  $x_i$ —a point of the trajectory ( $i = 1, \dots, N$ ),  $y_j$ —a point of the trajectory ( $j = 1, \dots, M$ ),  $\| \cdot \|$ —the norm in  $m$ -dimensional space.

The CRP shows all systems states in which points on the trajectory of one dynamical system are close to points on the trajectory of the other dynamical system. If the distance between points  $x_i$  and  $y_j$  is less than or equal to  $\varepsilon$ , then  $CRP_{i,j} = 1$ , otherwise  $CRP_{i,j} = 0$ . In Fig. 4 the examples of CRPs calculated based on the pixel brightness changes (sum) in two neighboring minichannels (1 and 2) are shown. For a higher water flow rate (Fig. 4b), a higher density of CRP is observed. In Fig. 4a, b the processes observed in both gates are

very dynamic, states with only liquid or only vapor occur rarely in the gates. The recurrence in this case is calculated between different phase distributions in the gates. For water flow rate equal to 570 g/h (Fig. 4c) the CRP is almost completely blackened. This is related to a very high content of liquid inside minichannels. In this case the recurrence is related to the occurrence of only one phase in both gates, the dynamics of phase change is low. Thus, further cross recurrence analysis of pixel brightness will be performed for  $\dot{m} < 400$  g/h. A quantitative evaluation of CRPs is performed using the cross recurrence quantification analysis (CRQA) [12].

Diagonal cross recurrence profile (DCRP) [14] is a type of CRQA analysis. This method is limited to the analysis of diagonal lines visible on the CRP. The most important coefficient used in DCRP analysis is the recurrence rate (RR), calculated using the following formula [12]:

$$RR(t) = \frac{1}{N - |t|} \sum_{l=1}^{N-|t|} lP_t(l), \tag{2}$$

where  $t$  is the characteristic time shift defining the distance from the diagonal line (LOS),  $P_t(l)$  is the histogram of the  $l$ -length continuous diagonal lines ( $t = 0$  denotes the main diagonal line called also as the line of synchronization—LOS).

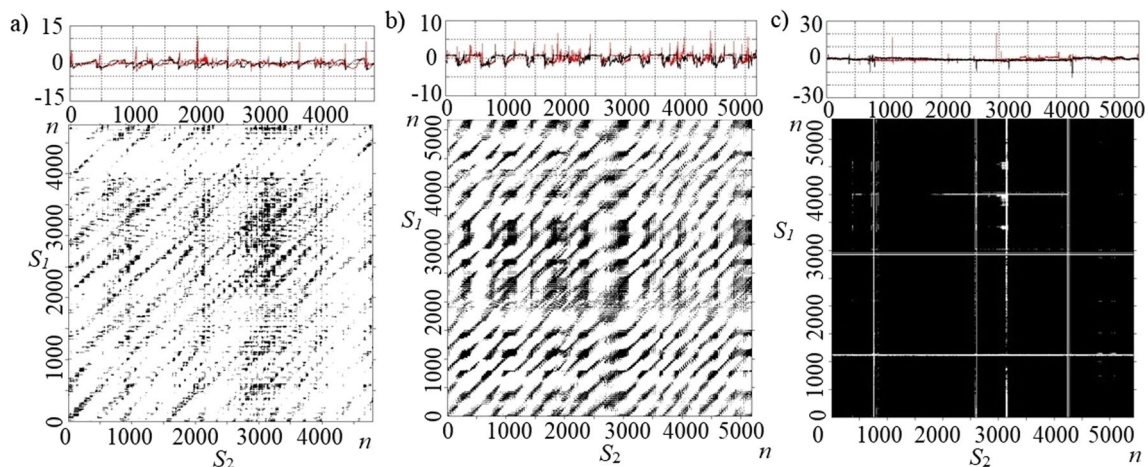


**Fig. 4** The example of CRPs of visual data registered during flow boiling for: **a**  $\dot{m} = 175$  g/h ( $m = 6, \tau = 84$ ); **b**  $\dot{m} = 316$  g/h ( $m = 7, \tau = 32$ ); **c**  $\dot{m} = 537$  g/h ( $m = 6, \tau = 7$ ). The CRPs were performed using a CRP MATLAB Toolbox ( $\varepsilon = 15\%d$ )



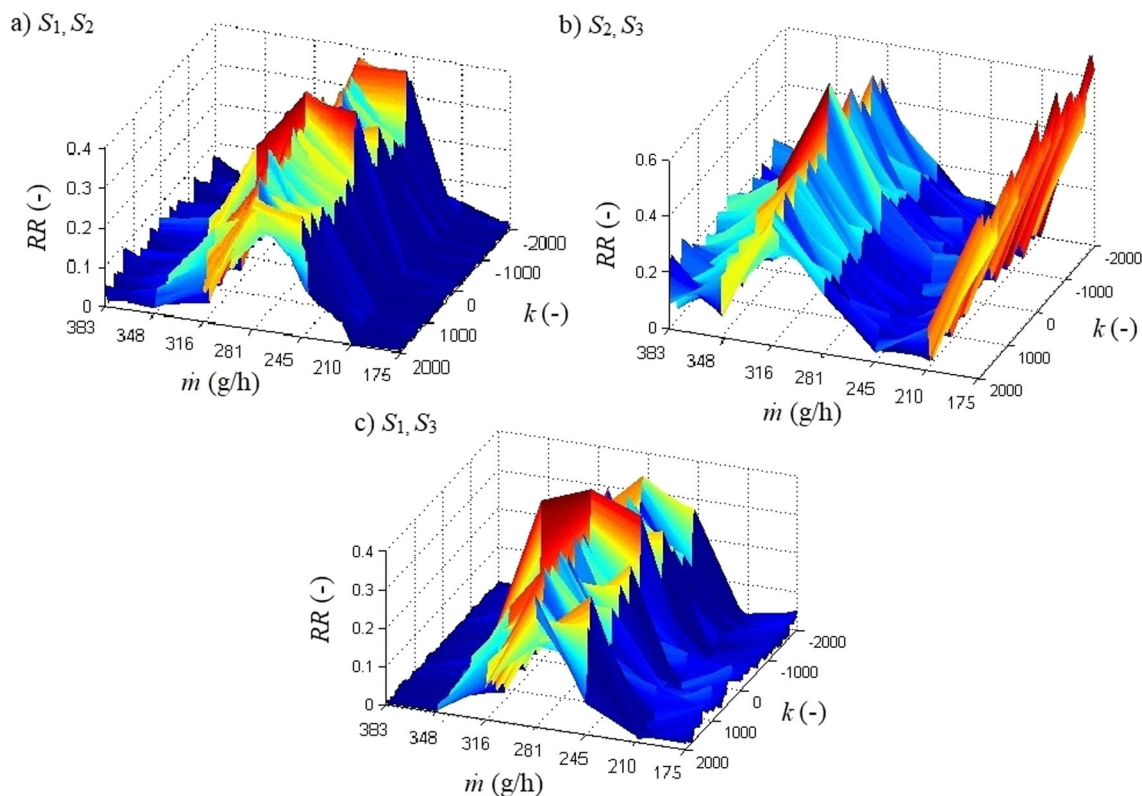


**Fig. 5** The RR functions based on the CRPs of pixel brightness changes in neighboring minichannels: **a**  $S_1, S_2$ , **b**  $S_2, S_3$ , **c**  $S_1, S_3$  vs. water flow rate ( $\dot{m}$ ) obtained for 4000 diagonal lines,  $k = \{-2000, 2000\}$

The RR coefficient is used to calculate the number of recurrence points on diagonal lines. The analysis carried out in this way allows to obtain a graph of changes of the RR coefficient as a function of the lag,  $t$ , which has been called diagonal cross recurrence profile. The highest synchronization between both time series is observed for lag = 0 and for the highest RR.

Figure 5 presents RR functions vs. water flow rates and  $k = 4000$  diagonal lines (lags). The analysis of RR function vs. water flow rates was performed for  $\dot{m} < 400$  g/h. Figure 5a shows RR functions for minichannels 1 and 2, Fig. 5b for minichannels 2 and 3 and Fig. 5c for minichannels 1 and 3. The functions of RR obtained for two pairs of minichannels: 1 and 2 and 1 and 3 are very similar (Fig. 5a, c). For water flow rates in the range of 210–281 g/h the RR function increases—similar flow patterns and flow dynamics are identified in minichannels. The maximum of RR for both those pairs of minichannels (1 and 2, 1 and 3) is observed for  $\dot{m} = 281$  g/h and it indicates flow boiling synchronization in the analyzed parts of minichannels. In this case, very intense flow boiling with reverse flow, long vapor slugs filling the minichannels and several small bubbles were observed (Table 1). A high content of vapor was filling minichannels. When flow boiling becomes less intense  $\dot{m} > 281$  g/h, the RR functions decrease. A lower value of RR corresponds to a change of two-phase flow patterns and flow dynamics in neighboring minichannels. Figure 5b represents an analysis of synchronization between minichannels 2 and 3.

During very intense boiling  $\dot{m} = 175$ – $210$  g/h the first maximum of RR function is observed ( $\dot{m} = 175$  g/h). The second maximum of RR function is shifted towards flows with slightly higher water flow rate ( $\dot{m} = 316$  g/h) than in the case of minichannels 1 and 2 and 1 and 3 (Fig. 5a, c). The maximum value of RR is also higher than in Fig. 5a and c. This indicates that the highest boiling synchronization is observed between minichannels 2 and 3. We can suppose, that flow between those minichannels may be influenced by an intense and periodic movement of RFB which is described in Sect. 2. The maximum values of RR in Fig. 5 occur mostly for lag = 0, but also for different values of lags. This is caused by the fact, that the highest synchronization was observed in the gates when short slug flow occurred. If a vapor slug was longer than the length of the gate, then the maximum of RR was observed for different time lags (not only for lag = 0). This is also visible based on CRPs in Fig. 4 where the diagonal lines are not parallel to the main diagonal line, so the analysis based on time lags is not always clear.

The DCRP analysis of pixel brightness changes inside minichannels has been applied to identify the similarity of flow patterns changes inside minichannels. However, we lack information considering flow synchronization between inlet and outlet pressure fluctuations. Moreover, in the paper [15] authors have stated that the analysis of pressure distribution can be a potentially effective method for detecting flow maldistribution and its intensity. Thus, we have performed a DCRP analysis

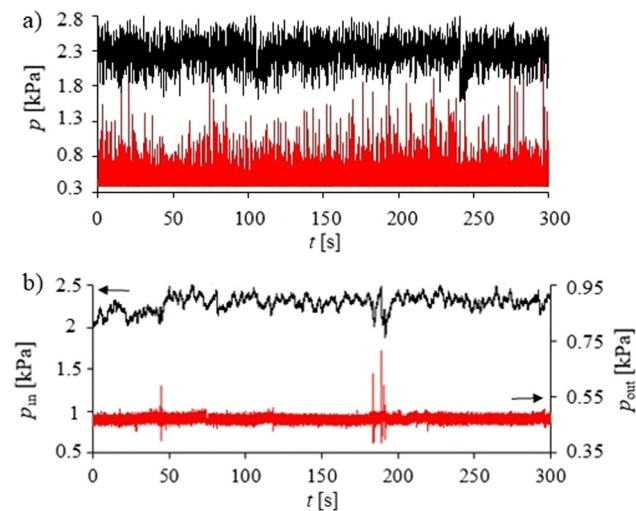


**Fig. 6** Pressure oscillations recorded at the inlet (black color) and outlet (red color) of the minichannels: **a**  $\dot{m} = 316$  g/h ( $\sigma_{p_{in}} = 0.17$ ,  $\sigma_{p_{out}} = 0.16$ ), **b**  $\dot{m} = 570$  g/h ( $\sigma_{p_{in}} = 0.08$ ,  $\sigma_{p_{out}} = 0.01$ )

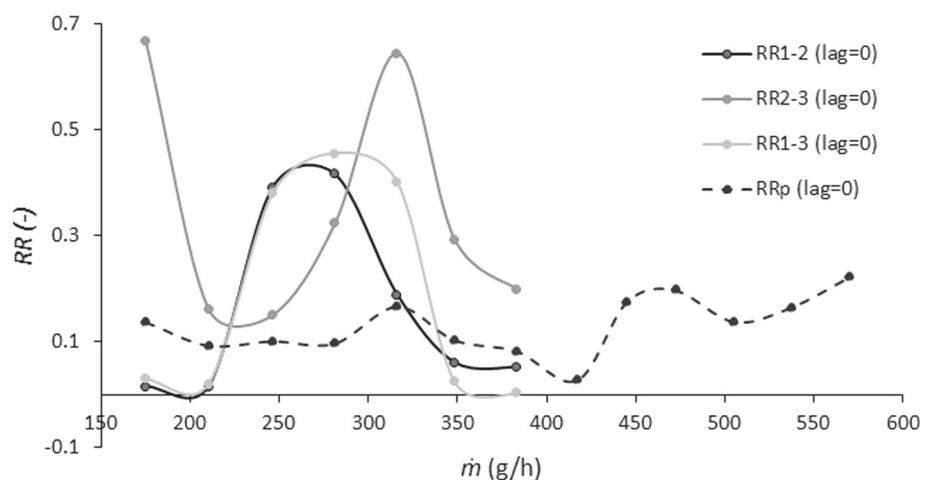
of pressure oscillations recorded at the inlet and outlet common area.

## 2.2 Pressure analysis

In order to assess flow synchronisation between inlet and outlet common area we analysed pressure oscillations recorded at the inlet and outlet of the minichannels. The pressure oscillations registered at different water flow rates were used for the DCRP analysis. Each signal has been normalized before the analysis. Then, the CRPs were created. Two examples of analysed pressure signals are shown in Fig. 6. Additionally, a standard deviation of the inlet pressure ( $\sigma_{p_{in}}$ ) and outlet pressure ( $\sigma_{p_{out}}$ ) was calculated and included in Fig. 6 capture. The standard deviation of inlet and outlet pressure oscillations is much higher during intense boiling (Fig. 6a).

The parameters  $m$ ,  $\tau$  and  $\varepsilon$  for the CRP analysis were determined for the pressure oscillation signal recorded at the inlet to the minichannels. The value of  $\varepsilon$  was

**Fig. 7** The RR coefficient (DCRP analysis) for main diagonal line (lag = 0) for pixel brightness changes in minichannels (RR1-2, RR2-3, RR1-3) and for inlet and outlet pressure drop signal (RRp) vs. water flow rates ( $\dot{m}$ )



equal to 15% of the maximum attractor diameter. The  $m$  value was estimated using the false nearest neighbors method [16]. The value of  $\tau$  was determined using the mutual information method [16]. All diagonal lines appearing on the CRPs were quantified by the RR coefficient which was calculated using DCRP function from the CRP package in MATLAB.

Figure 7 shows RR coefficient for main diagonal line (lag = 0) calculated based on image analysis (RR1-2, RR2-3, RR1-3) and based on inlet and outlet pressure fluctuations (RRp).

## 3 Conclusions

In Fig. 7, the RR coefficient changes for the main diagonal line for analyzed water flow rates was presented. The greatest synchronization of pixel brightness changes in two pairs of minichannels (1–2 and 1–3) was observed for water flow rates in the range of 246–350 g/h. For minichannels 2–3 the amplitude of RR is much higher and the peak is observed for water flow rates in the range of 280–350 g/h. This indicates the highest boiling synchronization observed between minichannels 2 and 3. The asymmetry in this case was observed in the geometry of the setup which affected the movement of the ‘reverse flow bubble’ in the inlet common plenum. The RR coefficient calculated between inlet and outlet pressure signal (RRp, lag = 0) has its first peak for water flow rates in the range of 280–350 g/h. This corresponds to the high boiling synchronization observed for minichannels 2 and 3 which was influenced by RFB movement.

In order to assess the flow stability during high boiling synchronization the standard deviation of inlet and outlet temperature and pressure was calculated and presented in Fig. 8.

The highest synchronization of phase distribution during flow boiling was identified for water flow rates from 280 g/h up to 350 g/h (Fig. 7). The beginning of the synchronization is closely related to reverse flow

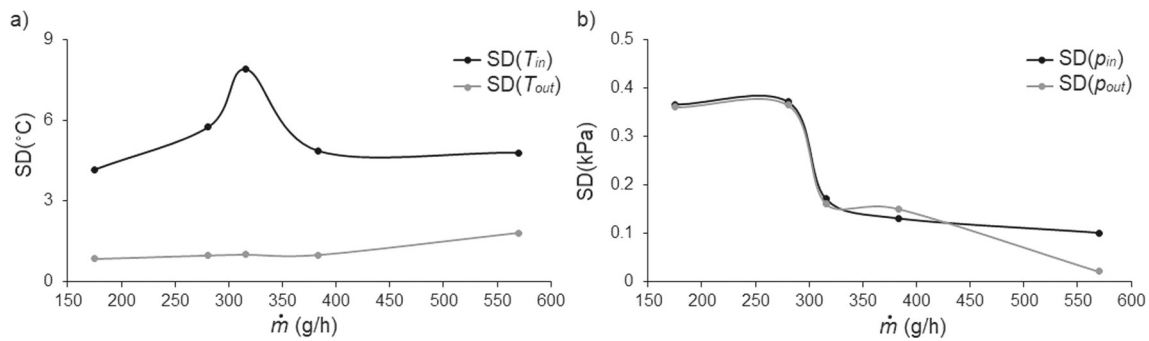


**Fig. 8** The standard deviation of boiling parameters registered at  $\dot{m} = 175$  g/h,  $\dot{m} = 281$  g/h,  $\dot{m} = 316$  g/h,  $\dot{m} = 383$  g/h,  $\dot{m} = 570$  g/h: **a** inlet and outlet temperature (SD( $T_{in}$ ), SD( $T_{out}$ )), **b** inlet and outlet pressure (SD( $p_{in}$ ), SD( $p_{out}$ ))

and *RFB* movement as the standard deviation of inlet temperature and pressure is the highest (Fig. 8). It can be concluded that the processes of synchronization have a negative impact on temperature and pressure oscillations. During synchronization processes an increase in temperature and pressure oscillations is observed—heat flux decreases, the heat exchange is not uniform [6, 8]. With the increase in water flow rate, reverse flow occurs more rarely, the oscillations of water inlet temperature decrease, the standard deviation of inlet pressure decreases. The oscillations of the outlet temperature and outlet pressure decrease—the process of boiling is becoming less intense, it is less likely to generate reverse flow. The decrease in synchronization (lack of synchronization) causes a decrease in the intensity of reverse flows. The results show that recurrence analysis of inlet and outlet pressure oscillations can be used for assessment of boiling synchronization in minichannels.

**Acknowledgements** This work was supported by the National Science Centre, Poland [Grant number: UMO-2017/27/B/ST8/02905]. This work was supported by the science work number WI/WM-IIM/6/2021 and financed from a research subsidy provided by the Minister of Education and Science.

**Open Access** This article is licensed under a Creative Commons Attribution 4.0 International License, which permits use, sharing, adaptation, distribution and reproduction in any medium or format, as long as you give appropriate credit to the original author(s) and the source, provide a link to the Creative Commons licence, and indicate if changes were made. The images or other third party material in this article are included in the article's Creative Commons licence, unless indicated otherwise in a credit line to the material. If material is not included in the article's Creative Commons licence and your intended use is not permitted by statutory regulation or exceeds the permitted use, you will need to obtain permission directly from the copyright holder. To view a copy of this licence, visit <http://creativecommons.org/licenses/by/4.0/>.

**Data availability statement** The data that support the findings of this study are not openly available due to large

amount of the processes data and are available from the corresponding author upon reasonable request in a controlled access repository where relevant.

### Declarations

**Conflict of interest** The authors have no competing interests to declare that are relevant to the content of this article.

### References

1. Q. Jin, J.T. Wen, S. Narayanan, *Int. J. Therm. Sci.* **156**, 106476 (2020)
2. H. Grzybowski, I. Gruszczyńska, and R. Mosdorf, *MATEC Web of Conferences* **240**, (2018).
3. G. Rafałko, I. Zaborowska, H. Grzybowski, R. Mosdorf, *Energies* **13**, 1409 (2020)
4. H. Grzybowski, R. Mosdorf, *Int. Commun. Heat Mass Transfer* **95**, 25 (2018)
5. I. Zaborowska, *Int. J. Heat Mass Transf.* **10** (2021).
6. S.H. Yoon, N. Saneie, Y.J. Kim, *Int. J. Heat Mass Transf.* **78**, 527 (2014)
7. A. Marchitto, F. Devia, M. Fossa, G. Guglielmini, C. Schenone, *Int. J. Multiph. Flow* **34**, 128 (2008)
8. S.G. Kandlikar, Z. Lu, W.E. Domigan, A.D. White, M.W. Benedict, *Int. J. Heat Mass Transf.* **52**, 1741 (2009)
9. C.J. Ho, P.-C. Chang, W.-M. Yan, P. Amani, *Int. J. Heat Mass Transf.* **122**, 264 (2018)
10. S. Wallot and G. Leonardi, *Front. Psychol.* **9** (2018).
11. G. Rafałko, H. Grzybowski, P. Dzieńis, R. Mosdorf, A. Adamowicz, *Chem. Eng. Technol.* **44**, 1978 (2021)
12. N. Marwan, J. Kurths, *Phys. Lett. A* **302**, 299 (2002)
13. N. Marwan, J. Kurths, *Math. Phys. Res. Cutting Edge* **101** (2004).
14. R. Dale, N. Kirkham, D. Richardson, *Front. Psychol.* **2** (2011).
15. M. Klugmann, P. Dabrowski, D. Mikielawicz, *Arch. Thermodyn.* **39**, 123 (2018)
16. H. Kantz, T. Schreiber, *Nonlinear Time Series Analysis*, 2nd edn. (Cambridge University Press, Cambridge, 2003)